



AT 2020iko: A WZ Sge-type Dwarf Nova Candidate with an Anomalous Precursor Event

Monika D. Soraisam^{1,2}, Sarah R. DeSantis³, Chien-Hsiu Lee⁴, Thomas Matheson⁴, Gautham Narayan², Abhijit Saha⁴, David J. Sand³, Carl Stubens⁴, Paula Szkody⁵, Nicholas Wolf⁴, Samuel D. Wyatt³, Ryohei Hosokawa⁶, Nobuyuki Kawai⁶, and Katsuhiko L. Murata⁶

¹ National Center for Supercomputing Applications, University of Illinois at Urbana-Champaign, Urbana, IL 61801, USA; soraisam@illinois.edu

² Department of Astronomy, University of Illinois at Urbana-Champaign, Urbana, IL 61801, USA

³ Steward Observatory, University of Arizona, 933 North Cherry Avenue, Tucson, AZ 85721, USA

⁴ NSF's National Optical-Infrared Astronomy Research Laboratory, 950 North Cherry Avenue, Tucson, AZ 85719, USA

⁵ University of Washington, Department of Astronomy, Box 351580, Seattle, WA 98195, USA

⁶ Tokyo Institute of Technology, 2 Chome-12-1 Ookayama, Meguro City, Tokyo 152-8550, Japan

Received 2020 August 6; revised 2020 October 23; accepted 2020 October 26; published 2020 December 7

Abstract

The ongoing Zwicky Transient Facility (ZTF) survey is generating a massive alert rate from a variety of optical transients and variable stars, which are being filtered down to subsets meeting user-specified criteria by broker systems such as the Arizona-NOIRLab Temporal Analysis and Response to Events System (ANTARES). In a beta implementation of the algorithm of Soraisam et al. on ANTARES, we flagged AT 2020iko from the ZTF real-time alert stream as an anomalous source. This source is located close to a red extended Sloan Digital Sky Survey source. In the first few epochs of detection, it exhibited a V-shaped brightness profile, preceded by nondetections both in ZTF and in the All-Sky Automated Survey for Supernovae extending to 2014. Its full light curve shows a precursor event, followed by a main superoutburst and at least two rebrightenings. A low-resolution spectrum of this source points to a dwarf nova (DN) nature. Although some of the features of AT 2020iko indicate an SU UMa-type DN, its large amplitude, presence of rebrightenings, and inferred supercycle period of ≥ 6 yr are in favor of AT 2020iko being a new WZ Sge-type DN candidate, a subset of rare DNe consisting of extreme mass-ratio (< 0.1) binaries with an orbital period around the period minimum. The precursor event of AT 2020iko brightened by 6.5 mag, while its decay spanned 3–5 mag. We speculate this superoutburst is associated with a less expanded accretion disk than in typical superoutbursts in WZ Sge systems, with the large depth of the precursor decay implying an extremely small mass ratio. To the best of our knowledge, such a precursor event has not been recorded for any DN. This result serves to demonstrate the efficacy of our real-time anomaly search algorithm.

Unified Astronomy Thesaurus concepts: Dwarf novae (418); WZ Sagittae stars (1809); Time domain astronomy (2109)

Supporting material: machine-readable table

1. Introduction

Current wide-field sky surveys are boosting the density of, and even occasionally populating, the parameter space of observed astrophysical sources. The Zwicky Transient Facility (ZTF; Bellm et al. 2019) is a leader in optical time-domain astronomy. ZTF is surveying the entire visible northern sky using a CCD camera with a 47 deg² field of view fitted to the 48 inch Samuel Oschin Schmidt Telescope at the Palomar Observatory. Alerts, i.e., detections of flux- or position-varying sources at a signal-to-noise ratio (S/N) ≥ 5 (Masci et al. 2019), from the public part of ZTF (comprising 40% of observing time) are being streamed to event brokers (Patterson et al. 2019). The latter are software systems that add values to alerts, custom-filter them to a manageable level, and deliver them to the users near real time; examples include the Arizona-NOIRLab Temporal Analysis and Response to Events System (ANTARES; Saha et al. 2016; Matheson et al. 2020), AMPEL (Nordin et al. 2019), LASAIR (Smith et al. 2019), the Automatic Learning for the Rapid Classification of Events (ALeRCE; Förster et al. 2020), and MARS.⁷

An important goal of the real-time delivery of (filtered) alerts is to facilitate discovery and characterization of the nature, via follow-up observations, of relatively rare (e.g., in terms of rate)

short-lived sources. Algorithms aimed toward such discoveries for astronomical time-series data have been developed (e.g., Giles & Walkowicz 2019; Ishida et al. 2019; Soraisam et al. 2020b). In this paper, we present the discovery and multi-wavelength follow-up results of a new WZ Sge-type dwarf nova (DN) candidate, from a beta implementation of such an algorithm in the real-time alert environment.

Dwarf novae are a subclass of cataclysmic variables (CVs) comprising an accreting white dwarf (WD) in a binary system with typically a late-type main-sequence companion, whereby the WD undergoes semiregular outbursts (Warner 2003). The most widely studied theoretical model for the DN outbursts invokes a thermal instability in the accretion disk, which acts to increase the viscosity (parameterized by α ; Shakura & Sunyaev 1973) resulting in a runaway increase of the disk temperature and mass accretion onto the WD, which, in turn, transforms the accretion disk to a cool state, and the cycle repeats (e.g., Smak 1971; Meyer & Meyer-Hofmeister 1981; Osaki 1996; Lasota 2001; Hameury 2020). The DN outbursts are a common phenomenon, accounting for the majority of the observed optical transients or stochastic variable stars in the Galaxy in current synoptic time-domain surveys (e.g., Szkody et al. 2020). These objects have provided significant insights into the properties of accreting WDs, in particular their

⁷ <https://Mars.lco.global>

accretion disks, and the evolution and population of low-mass stellar binaries (Pala et al. 2020).

Photometrically, DN outbursts are often characterized by an amplitude of several magnitudes ($\sim 2\text{--}5$ mag) lasting for a few days and recurring on timescales of months. However, there is a rarer subclass called WZ Sge-type DNe, which show a larger-amplitude (reaching up to ~ 9 mag) superoutburst lasting for week(s), superposed with periodic fluctuations (called superhumps), multiple rebrightenings, and a long recurrence period on the order of a decade or more (Kato 2015). They are at the extreme tail of SU UMa-type DNe, which show both normal and superoutbursts recurring on a timescale of typically a few months. For the following, the reader should keep in mind this subclass relation whenever aspects of either class of systems are discussed.

WZ Sge-type systems have a short orbital period, close to the period minimum (~ 80 minutes), a very low value of the viscosity parameter during quiescence α_{cold} , and a highly asymmetric mass ratio with the donor star mass less than one-tenth of that of the WD (Smak 1993; Osaki & Meyer 2002 and references therein). Their early phase (within the first 10 days or so of the outburst) superhumps correlate with the orbital period of the system—the inclination-dependent photometric manifestation of tidal dissipation of angular momentum resulting from the 2:1 resonance between the accretion disk and the orbital motion in close binaries with extreme mass ratios (e.g., Lin & Papaloizou 1979). Their later-phase superhumps, on the other hand, have a period that is slightly longer than the orbital period, and are related to the precession of the tidally deformed eccentric disk excited at the 3:1 resonance radius, common across SU UMa-type DNe (Whitehurst 1988).

Although the number of WZ Sge-type DNe detected has significantly increased with the advent of wide-field surveys, they remain relatively rare, with their discovery rate being a few tens per year (Kato 2015). For comparison, there are, for example, a few hundred type Ia supernovae detected per year. This is likely due to the fact that dedicated supernovae searches covering large areas with good enough cadence are quite popular, while there are no dedicated searches with proper cadences for such DNe. Next-generation wide-field surveys, specifically Rubin Observatory’s Legacy Survey of Space and Time (LSST; Ivezić et al. 2019), have the potential to discover many such transients, particularly opening up the faint-magnitude space. However, its main survey component, namely the Wide-Fast-Deep survey, which is currently baseline to a sampling cadence of around 10–20 days per passband (LSST Science Collaboration et al. 2017) is not ideal to detect and characterize fast-evolving outbursts from CVs. Specialized mini-surveys focusing on the Galactic plane or a few nearby galaxies with a much higher cadence (e.g., deep-drilling-like; LSST Science Collaboration et al. 2017), which have been proposed, would be more favorable to this end.

This paper is organized as follows. Section 2 outlines the discovery of our source, while the follow-up observations are detailed in Section 3. We discuss the observation results in Section 4 and conclude with Section 5.

2. Anomaly Transient Selection

We have implemented a real-time filter on ANTARES based on the algorithm of Soraisam et al. (2020b) to flag peculiar astrophysical sources from the ZTF alert stream. To this end,

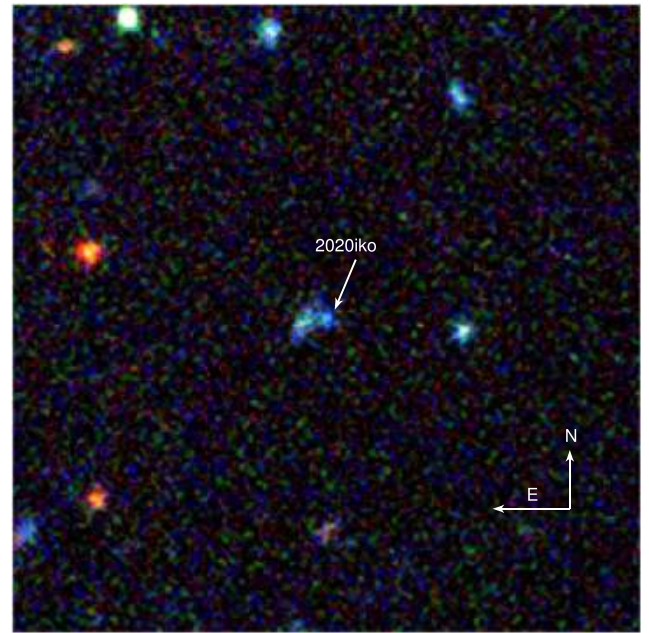


Figure 1. Color cutout image ($1' \times 1'$) of 2020iko (indicated by the white arrow) from the legacy surveys. An extended source is also visible immediately to the east (i.e., left) of 2020iko.

we use a sample of tens of thousands of persistent variable sources from ZTF, whose labels are obtained from cross-matching with external catalogs in the ANTARES processing. The relevant catalogs include those of the All-Sky Automated Survey for Supernovae (ASAS-SN) variable stars (Jayasinghe et al. 2018) and quasars and active galactic nuclei (AGNs; Véron-Cetty & Véron 2010). We use the ZTF light curves of these variable sources to construct the conditional probabilities of magnitude changes and pseudocolors for given time intervals. These distributions are used to evaluate the likelihood score of consistency with this population of variable sources for any newly detected alert (see Soraisam et al. 2020b for details).

ZTF20aawbodq (AT2020iko, hereafter 2020iko) was flagged with one of the lowest likelihood scores, thus denoting a peculiar candidate (Soraisam et al. 2020a). The source is located at (J2000) R.A. = 09:03:26.23 decl. = +47:31:59.14 ($l = 172.12759$, $b = 41.57730$), within $0''.5$ of the extended Sloan Digital Sky Survey (SDSS) source J0903+4731 (Alam et al. 2015). This appears in line with the ZTF r -band nearest neighbor from the deep reference image (used in difference imaging) at a distance of $1''.83$ (less than the typical seeing of $2''$ for ZTF) from 2020iko, a magnitude of 22.89, and a star-galaxy score of 0.4 indicating extendedness.⁸ There is no g -band nearest neighbor in the ZTF data within $2''$. Given the close proximity to the extended source SDSSJ0903+4731, we initially suspected 2020iko to be an extragalactic transient.

Examining deeper images along with their source catalog from the recent eighth data release of the DESI Legacy Imaging Surveys (Dey et al. 2019), we find two sources around the position of 2020iko, for which a cutout of the color (g , r , z) image stack is shown in Figure 1. Out of the two, one is a point-like source at a distance of $0''.71$ from the ZTF location of 2020iko with magnitudes of $g = 23.27$, $r = 23.27$, and $z = 23.51$, and the other is an extended source at a distance

⁸ The ZTF alert data for 2020iko are accessible at <https://antares.noirlab.edu/loci/ANT2020ea3ig>.

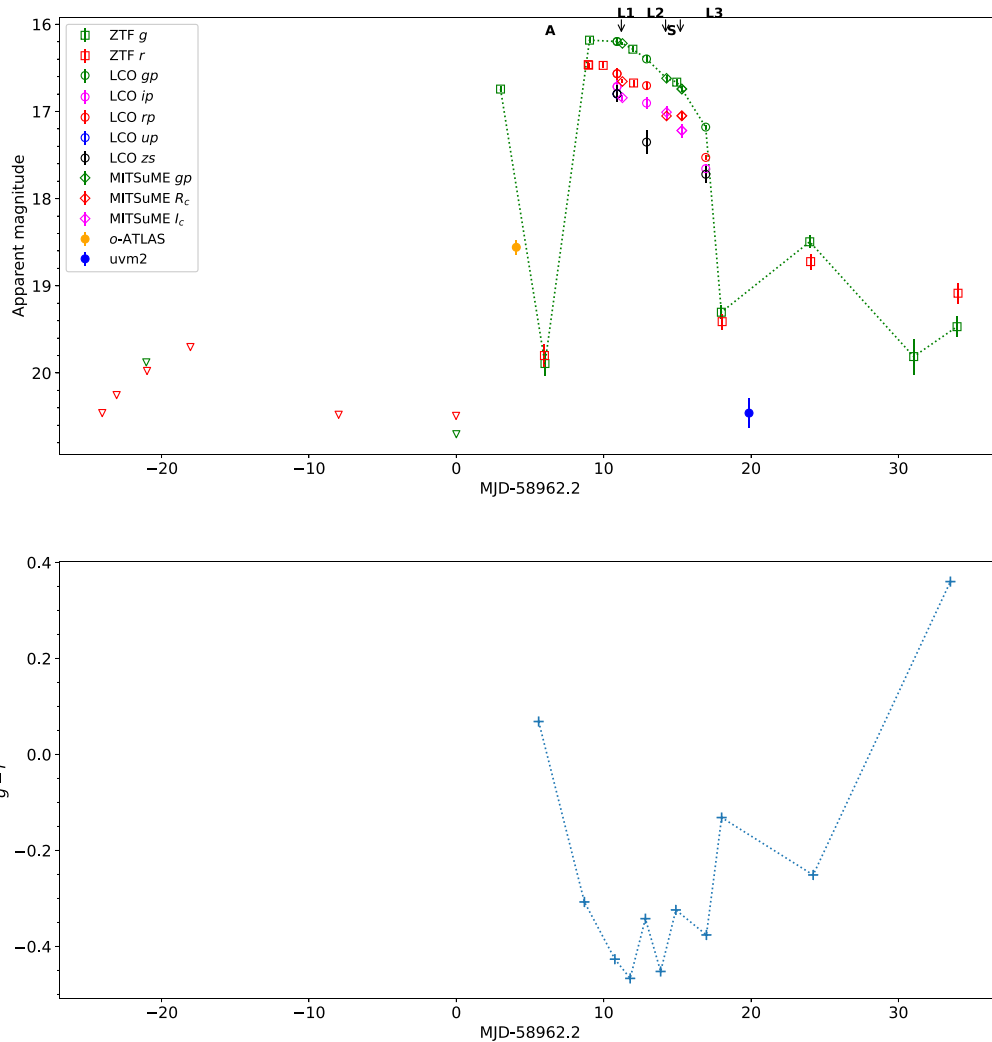


Figure 2. Top: light curve of 2020iko aggregating the measurements from ZTF, ATLAS, LCO, MITSuME, and Swift, as indicated by the legend. The LCO observations from the three nights, indicated by L1, L2, and L3, as well as the MITSuME observations indicated by the arrows are shown zoomed-in in Figure 3. Triangles denote the upper limits from ZTF in the *g* (green) and *r* (red) passbands. “A” marks the epoch when the source was flagged by our anomaly filter, and S, the epoch of spectroscopic observation (Section 3.4). The time axis is shown relative to the epoch of latest ZTF upper limit. The green dotted line connects the green data points and is meant to guide the eye regarding the evolution of the outburst. Note that the error bars are much smaller than the symbols for many of the data points. Bottom: color ($g - r$) evolution of 2020iko.

of $1''.75$ with magnitudes of $g = 23.0$, $r = 22.26$, and $z = 21.85$. Thus, the closer point source, which is marked with the arrow in Figure 1 and is slightly fainter than the extended source, is likely the progenitor of 2020iko.

The aggregated light curve of 2020iko is shown in Figure 2, which includes data from ZTF, the Asteroid Terrestrial-impact Last Alert System (ATLAS; Tonry et al. 2018), as well as follow-up observations (see Section 3). Table 1 lists all the photometric measurements. Our filter first flagged this source around MJD 58968 corresponding to the sharp decline of ~ 3 mag in 3 days. The public ZTF survey first detected it on 2020 April 26 UT (MJD 58965), at $g = 16.74$, preceded by nondetections, latest of which was on 2020 April 23 UT (MJD 58962) used as the time offset in Figure 2. Overall, the complete light curve seems to exhibit three features—a precursor decline, a main outburst with a plateau-like profile, and post-outburst rebrightenings—reminiscent of DNe as discussed above.

3. Follow-up

We initiated optical photometric and spectroscopic follow-up observations with the Las Cumbres Observatory (LCO; Brown et al. 2013) and Multicolor Imaging Telescopes for Survey and Monstrous Explosions (MITSuME; Kotani et al. 2005) facilities, as well as high-energy observations with Swift (Gehrels et al. 2004).

3.1. LCO Photometry

We performed multiwavelength follow-up observations using the Sinistro imager on the LCO 1 m telescope at the McDonald Observatory on three nights—UT May 4 (MJD 58973), May 6 (MJD 58975; TOM2020A-012; PI: Lee), and May 10 (MJD 58979; TOM2020A-011; PI: Narayan), labeled as L1, L2, and L3, respectively, in Figure 2. The exposure times for the different passbands (*gp*, *rp*, *ip*, and *zs*)⁹ per image are (3 s, 3 s, 3 s, and 10 s) on epoch L1, and (10 s, 10 s, 10 s,

⁹ The *up*, *gp*, *rp*, *ip*, and *zs* filters on the LCO Sinistro camera correspond to those of SDSS/Pan-STARRS.

Table 1
Light-curve Data

MJD	Source	Passband	Mag	Mag_error
58965.200903	ZTF	<i>g</i>	16.74	0.03
58966.271000	ATLAS	<i>o-ATLAS</i>	18.56	0.09
58968.180278	ZTF	<i>r</i>	19.80	0.14
58968.216215	ZTF	<i>g</i>	19.89	0.14
58971.151817	ZTF	<i>r</i>	16.46	0.03
58971.180544	ZTF	<i>r</i>	16.47	0.03
58971.239954	ZTF	<i>g</i>	16.18	0.03
58972.166701	ZTF	<i>r</i>	16.47	0.03
58973.106501	LCO	<i>gp</i>	16.18	0.08
58973.106852	LCO	<i>gp</i>	16.26	0.08
58973.107196	LCO	<i>gp</i>	16.16	0.07
58973.107647	LCO	<i>rp</i>	16.53	0.11
58973.107990	LCO	<i>rp</i>	16.56	0.12
58973.108341	LCO	<i>rp</i>	16.61	0.12
58973.108756	LCO	<i>ip</i>	16.62	0.13
58973.109092	LCO	<i>ip</i>	16.69	0.14
58973.109435	LCO	<i>ip</i>	16.91	0.17
58973.109886	LCO	<i>up</i>	16.82	0.10
58973.110315	LCO	<i>up</i>	16.62	0.12
58973.110730	LCO	<i>up</i>	16.90	0.10
58973.111259	LCO	<i>zs</i>	16.60	0.14
58973.111681	LCO	<i>zs</i>	16.86	0.17
58973.112096	LCO	<i>zs</i>	17.12	0.20
58973.455033	MITSuME	<i>R_c</i>	16.43	0.14
58973.455033	MITSuME	<i>gp</i>	16.18	0.12
58973.455033	MITSuME	<i>I_c</i>	16.67	0.19

(This table is available in its entirety in machine-readable form.)

and 15 s) on epochs L2 and L3. We also took a sequence of *up* exposures on epoch L1, each of 10 s. We collected a total of 3, 2, and 6 exposures per passband on L1, L2, and L3, respectively.

We obtained the BANZAI pipeline-reduced images from LCO (McCully et al. 2018) and used them to perform forced aperture photometry at the position of 2020iko. We calibrated the photometric results using PS1 measurements of sources in the same field (typically a few dozen), and SDSS measurements for the *up*-band. The zero-point errors are only a few millimagnitudes. The error-weighted average per passband for a given epoch is shown in the aggregated light curve (Figure 2). As evident from the plot, the LCO photometry data (particularly *gp* and *rp*) smoothly follow the plateau-like profile giving credence to our calibration.

The individual LCO measurements on each of these three nights are also expanded in Figure 3. As can be seen, the redder data points (particularly *zs*) are marred by large errors. However, a hint of coherent intranight variability can be seen mainly for *rp* and *ip* measurements (e.g., on epoch L3) at the level of 0.2 mag.

3.2. MITSuME Photometry

2020iko was also observed simultaneously in three passbands (*gp*, *R_c*, and *I_c*) with the MITSuME 0.5 m telescope at Akeno Observatory on three nights—UT May 4 (MJD 58973), May 7 (MJD 58976), and May 8 (MJD 58977), marked by the arrows in Figure 2. A sequence of 60 s exposures were taken on each of these nights. We performed photometry for these observations in a similar manner to that of the LCO data, and

the error-weighted average per passband for each night is shown in Figure 2.

For the MITSuME observations, we have a larger number of measurements per night than with LCO. We therefore bin them into 5 minute bins to reduce the measurement noise and the results are shown in Figure 3. A clear signature of intranight variability at a level of 0.2 mag (for *gp*) can be seen for the May 4 (MJD 58973) MITSuME observations with the longest intranight baseline of around 50 minutes. This interval is, however, smaller than the minimum orbital period of CV systems and therefore it is not sufficient to perform period analysis, which requires covering of at least 1.5 cycles for any meaningful inference. Nevertheless, the variability level matches the typical amplitude of superhump variability (Section 4).

3.3. Optical Color Evolution

We also compute the color evolution using *g/gp* and *r/rp/R_c* data points. We bin the light curve into 1 day bins, and take the mean magnitude in a given passband if there is more than one measurement. It is to be noted that the photometric measurements of ZTF are obtained from difference images, where the extended red source in the background has been subtracted (assuming it does not vary). For the follow-up observations, the photometry is performed without image subtraction. However, the extended source is very faint ($r \sim 22.3$ mag), and therefore it is not expected to significantly influence the color data points computed using those measurements, which were all taken around the bright plateau of the light curve. The result is shown in the bottom panel of Figure 2. The color has been corrected for foreground extinction using the reddening value of $E(B-V) = 0.026$ in the farthest-distance bin from the 3D reddening map of Green et al. (2018).

As can be seen, the source is quite red with $g-r \sim 0.1$ at the precursor minimum, but morphs to a blue color with $g-r \sim -0.3$ three days later at the observed peak of the main outburst. The emission continues to grow bluer in time during the gradually declining plateau in the light curve reaching $g-r \sim -0.45$, later fluctuating slightly at a level of around 0.1 mag, possibly related to incomplete phase coverage for the follow-up observations. This is immediately followed by a color inversion as the light curve drops sharply in brightness around MJD 58980, but later grows bluer again during the subsequent first rebrightening. The light curve seems to indicate a second rebrightening peak beyond the last epoch of observation by ZTF on MJD 58996 (see Section 4), where the color is the reddest ($g-r \sim 0.35$). Thus, the color trend of 2020iko can be summarized as bluer when bright and redder when faint.

During a DN outburst, the accretion disk is optically thick and its emission can thus be modeled with a blackbody with a radially varying temperature profile (Horne & Cook 1985). Assuming the optical emission to originate from the same outermost region, we can make a crude estimate of the evolution of the color temperature using Figure 2 (bottom panel). Noting that the passbands *g* and *r* do not have much constraining power at high temperatures when they are located at the Rayleigh–Jeans tail, we obtain a color temperature $>10^4$ K at $g-r \lesssim 0.1$, while at the reddest point, $g-r \sim 0.35$, during the rebrightening phase the color temperature is around 7500 K.

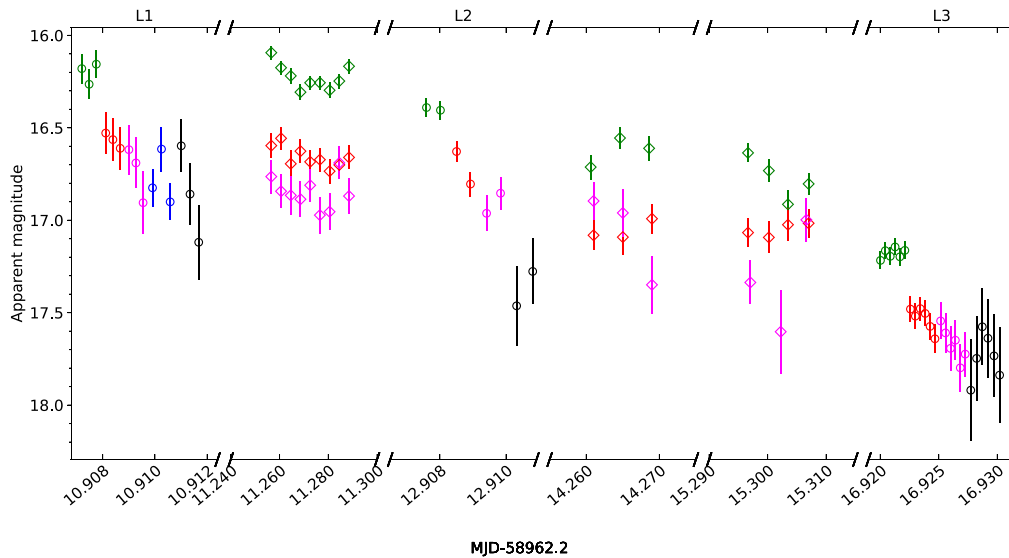


Figure 3. Light curve of 2020iko from follow-up LCO observations on the three epochs L1, L2, and L3, and MITSuME observations indicated by the arrows in Figure 2. The corresponding passbands of the data points are the same as shown in the legend of Figure 2. There were no *up* measurements on the last two LCO epochs, L2 and L3.

The overall color trend of 2020iko appears to be similar to observations of superoutbursts of other DN systems. For example, the 2001 superoutburst of the prototype WZ Sge with *UBVRI* observations showed a blue color during its initial superoutburst phase and a redder color during its decline, which later transitioned to a blue color again at its post-superoutburst rebrightening peak, though not as blue as during the superoutburst (see Howell et al. 2004). Based on the observed color temperatures, Howell et al. (2004) characterized the observed rebrightening of WZ Sge as a cyclical transition of the accretion disk from a neutral state to an ionized state. A similar behavior is also shown by the optical color, in particular, $V-R_c$, of another WZ Sge-type DN SDSS J102146.44+234926.3 (Uemura et al. 2008).

3.4. LCO Spectroscopy

We also obtained a spectrum of the source on 2020 May 7 UT (MJD 58976), with the cross-dispersed low-resolution Folded Low Order whYte-pupil Double-dispersed Spectrograph (FLOYDS) spectrograph of LCO, mounted on its 2 m telescope on the Haleakala Observatory (LCO2020A-006; PI: D. Sand). We used a slit width of $2''$ with an exposure time of 2700 s. As can be seen from Figure 2, 2020ko was brighter than 17 mag when the spectrum was taken. Hence, despite the large slit width, the observation is not expected to be affected by the faint ($\gtrsim 22$ mag) nearby extended source (see Section 2). LCO performs the data reduction automatically based on the pipeline of Valenti et al. (2014). The extracted wavelength- and flux-calibrated 1D spectrum of 2020iko delivered by the LCO pipeline is shown in Figure 4.

The source exhibits a blue continuum. Though the spectrum is quite noisy, distinct absorption features of higher-order Balmer lines, in particular $H\beta$ through $H\epsilon$, can be seen at $z = 0$, which are marked in the plot; no $H\alpha$ feature is, however, visible in the spectrum. There is an absorption feature around 4425 Å, near $H\gamma$, which we verified as likely an artifact due to the imperfect flattening in the blue side and not due to Ca I. The spectrum is, thus, typical of a DN during outburst, wherein the accretion disk transitions to a hot, optically thick state leading

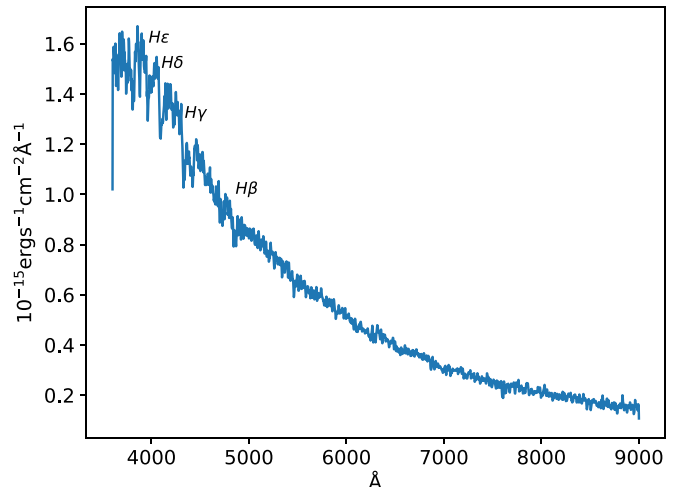


Figure 4. Optical spectrum of 2020iko observed with the LCO FLOYDS spectrograph. The spectrum has been smoothed using a running mean box kernel with a width of 3 pixels. The Balmer absorption lines are marked in the plot.

to the blue continuum and its absorption by the surface layers resulting in the Balmer absorption lines (e.g., Clarke et al. 1984; Szkody et al. 2002, 2003).

In addition to the blue continuum and Balmer absorption lines, emission lines of He II and C III/N III have been detected during the early outburst stage in WZ Sge-type DNe with the time-resolved spectra available (see Kato 2015, and references therein). Additionally, Na I D absorption line has been observed during the early stage in the prototype WZ Sge (Nogami & Iijima 2004) and during the rebrightening phase in EG Cnc (Patterson et al. 1998). These lines are not detected in the spectrum of 2020iko. However, its spectrum was obtained only during the late phase of its gradually declining plateau (Figure 2), which may explain the absence of these spectral features. The equivalent widths (EWs) of the higher-order Balmer absorption lines of 2020iko are around 5 Å each, slightly larger than the EWs of 2–3 Å for these lines observed around a similar stage for the superoutburst of the prototype

WZ Sge (Nogami & Iijima 2004). However, we consider them to be broadly consistent given the lower S/N of our spectrum and more importantly the poor spectral resolution of FLOYDS (ranging from 8.5 Å on the blue side to 17 Å on the red side), which make it difficult to determine precise EWs for 2020iko.

3.5. Swift Observations

We also requested a Swift ToO observation with the X-ray Telescope (XRT) and the UV/Optical Telescope (UVOT), which were executed about a week later on 2020 May 13 UT (MJD 58982) around the minimum of the decline of the main outburst. We analyzed the data using the Swift software package from HEASOFT. No X-ray emission was detected in an exposure of around 0.5 ks, and we obtained the 3σ upper limit on the count rate of $0.0267 \text{ counts s}^{-1}$ by running *sosta*. The source was, however, detected with the UVOT/*uvm2*. We used *uvotsource* to measure its magnitude, which is indicated by the blue filled circle in Figure 2. Apart from the fact that the source exhibited UV emission, the limited number of *uvm2* as well as *up* measurements are unconstraining, nevertheless we show them in the light curve for completeness.

4. Discussion

As mentioned in Section 1, one of the distinctive features for WZ Sge-type DNe (and generally SU UMa systems) is the presence of superhumps with amplitudes around 0.2–0.3 mag during the superoutbursts. Their detection requires extensive observations with minute-scale cadence, which, unfortunately, were not obtained for 2020iko. However, the few intranight observations (Figure 3) indicate a similar level of variability at around 0.2 mag.

Based on the counterpart for 2020iko in the deep legacy image (Section 2), we obtain an amplitude of 7.1 mag in the *g* band and 6.8 in the *r* band for its superoutburst. Its precursor outburst (Section 4.1) stands out with an amplitude of 6.5 mag in the *g* band. The duration of the superoutburst plateau is approximately 10 days, which is somewhat shorter than the typical duration of tens of days for WZ Sge-type DNe. Also, almost all such DNe show only superoutbursts with no precursors, which are, on the other hand, common for SU UMa-type systems. In WZ Sge systems, the outer edge of the accretion disk reaches the 2:1 resonance radius at the onset of a typical superoutburst. This radius serves as a tidal wall, where matter is dammed up due to very effective tidal removal of angular momentum from the disk (Osaki & Meyer 2003). Additionally, with the large mass accumulated during their long quiescence, the surface density at the tidal wall is well above the critical value (below which no hot state of the disk is possible) and the disk remains in the hot (outburst) state for a long duration. There is, thus, no time for a cooling wave to propagate to result in a precursor event in such systems. However, there are exceptions such as AL Com. This well-studied WZ Sge-type DN exhibited a superoutburst in 2015 that shares many common characteristics with 2020iko. Its plateau lasted ≈ 10 days and was preceded by a precursor (though not well separated; it is claimed to be the first precursor observed in any WZ Sge-type DNe) and showed a long post-superoutburst rebrightening (Kimura et al. 2016b). This particular superoutburst of AL Com was attributed to the limited expansion of the accretion disk, barely exceeding the

3:1 resonance radius and not reaching the 2:1 resonance radius at all.

Rebrightenings are typical in WZ Sge-type DNe, even though their underlying physical mechanism is not yet well understood. In fact, the light curve of 2020iko hints at a second rebrightening (Figure 2). The last ZTF alert from it was on 2020 May 27 UT (MJD 58996). By this time, the source was setting—it was already at an elevation $< 40^\circ$. Hence, it is most likely that the 2020iko field was not observed on subsequent nights, which prevented capturing additional rebrightening events.

Furthermore, to probe any possible historical outburst of 2020iko prior to ZTF, we queried the ASAS-SN database¹⁰ (Shappee et al. 2014; Kochanek et al. 2017) for its light curve since the start of the ASAS-SN survey. The baseline of ASAS-SN extends to 2014 with an average cadence of 2 days, covering a typical depth of $V \sim 17$ mag, which should be sufficient to detect at least the bright plateau phase of an outburst similar to that in Figure 2. However, no record of any historical outburst exists.

Taking all the above factors into account, we favor 2020iko to be a WZ Sge-type DN candidate with a superoutburst and a precursor (see below). Its superoutburst is, however, different from the typical superoutbursts in other WZ Sge-type systems, which are associated with the extension of the accretion disk beyond the 2:1 resonance radius (see Osaki & Meyer 2002). Instead, the underlying process in 2020iko’s superoutburst is likely similar to that of AL Com described above.

4.1. Significance of 2020iko’s Precursor

Some WZ Sge systems have been observed with a dip in brightness in the middle of their superoutburst, such as ASASSN-15jd (Kimura et al. 2016a) and SSS J122221.7–311523 (Kato et al. 2013). The duration of the pre-dip segment of the plateau for these systems is typically 10–20 days. The dip in these systems is attributed to the slow growth of the 3:1 resonance tidal instability following the end of the 2:1 resonance instability, which operates during the first segment. A cooling wave is, thus, able to propagate in the disk in the meantime, leading to a drop in the brightness. If we were to assume 2020iko to have a large dip in the middle of its superoutburst instead of a precursor, the duration of its first plateau segment would be at most 3–4 days (see Figure 2). To explain such a significantly shorter first segment would require some additional mechanism that can accelerate the removal of matter from the 2:1 resonance region. In the absence of such a mechanism, we instead consider this event in 2020iko to be a precursor outburst.

In the thermal tidal instability (TTI) model (Osaki 1996; Osaki & Meyer 2003), a superoutburst in SU UMa-type systems is triggered by a normal outburst. Depending on the final extension of the accretion disk during the precursor outburst and the growth rate of the resulting tidal instability, different time delays between the precursor and superoutburst are achieved. Many observed SU UMa-type systems show well-separated (i.e., 5–10 days) precursors to superoutbursts (for example, see Mróz et al. 2015 based on the Optical Gravitational Lensing Experiment observations; Osaki 2014 for V1504 Cyg and V344 Lyr; and Barclay et al. 2012 for NIK 1, the latter two works are based on Kepler data). Those

¹⁰ <https://asas-sn.osu.edu/>

precursors typically exhibit a decay of 1–1.5 mag.¹¹ On the other hand, precursors with much shallower decay (around 0.5 mag or less) appear merged with their superoutbursts, as shown by many SU UMa-type systems including TW Vir, SDSS 111236.7+002807 (Dai et al. 2016), CRTS J035905.9+175034 (Littlefield et al. 2018), and also some superoutbursts of V1504 Cyg and V344 Lyr (Wood et al. 2011; Osaki & Kato 2013; Osaki 2014; see also the theoretical models of Howell et al. 1995). Even the precursor to the 2015 superoutburst of AL Com (Section 4) belongs to this category. Hereafter we refer to the former type as normal precursors and the latter as merged precursors. The normal precursors are identical in amplitude to the normal outbursts¹² in the corresponding systems (Osaki & Meyer 2003; Osaki 2014), while the merged precursors exhibit a larger amplitude, though still $\lesssim 6$ mag.

In the high-cadence Kepler observations of V1504 Cyg and V344 Lyr, Osaki (2014) found that superhumps already appeared in the decay phase of their normal precursor outbursts, which then grew in amplitude with the development of the main outbursts. This is evidence in support of tidal instability powering these superoutbursts. The authors also found some normal outbursts with the same behavior, but with aborted superhumps (Osaki & Meyer 2003), which disappeared near quiescence, failing to excite a superoutburst.

As can be seen from Figure 2, the precursor of 2020iko has been caught in its decline—fading by 3 mag in 3 days. Following a 3 day gap, where there were no observations, the light curve shot up from its observed precursor minimum ($g \sim 20$) to the peak of its main outburst ($g \sim 16$), while the separation between the two observed peaks (i.e., of the precursor and superoutburst) is 6 days. Clearly it is not a merged precursor, but is it neither a normal precursor (see below). With a decline rate of 1 mag day⁻¹ for the precursor phase, it is unlikely this segment of the light curve faded to its progenitor magnitude of 23.27 (Section 2). Nevertheless, since the typical rise time for a superoutburst in DNe is around a day, it is possible for the precursor to have reached 22 mag, which would imply a deep decay of ~ 5 mag.

Despite the similarity in the light-curve morphology of 2020iko with SU UMa-type DN superoutbursts that show precursors, there are three main differences:

1. 2020iko has no recorded historical (normal or super) outbursts in >6 yr. This points to a very low value of the viscosity parameter α_{cold} for the cold accretion disk during quiescence, characteristic of WZ Sge systems (e.g., Smak 1993; Osaki 1995).
2. Its precursor has an amplitude of 6.5 mag (considering the rise to peak), which puts it in the realm of superoutburst amplitudes and makes it atypical for normal precursor outbursts. The amplitudes of the latter are in the range 1–2 mag.
3. Its precursor decay of 3–5 mag is an outlier among the superoutbursts of DNe with a precursor.

¹¹ One larger decay of 3 mag has been observed for V1504 Cyg with Kepler (Figures 1 and 3 of Osaki 2014), however these observations were heavily affected by noise, as described by Osaki (2014).

¹² Statistical studies of properties of CVs, for example, as conducted by Drake et al. (2014) show the distribution of outburst amplitudes extending to 8 mag. Though the CVs were not classified into subtypes, their orbital period distribution is concentrated at short orbital periods below the period gap. Thus, the CV outbursts in their sample are particularly biased toward superoutbursts, and hence the large amplitudes.

Kimura et al. (2020) recently presented observations of the 2018 superoutburst of EG Cnc, another well-known WZ Sge system, which was first caught during an initial decay in its light curve of around 2 mag (with a similar decline rate as 2020iko). There were no observations prior to the decay, which was deeper than its previous superoutburst in 1996–1997, whose first segment showed early superhumps. Otherwise, the 2018 event was identical to the 1996–1997 superoutburst. Kimura et al. (2020) interpreted this superoutburst as similar to that of ordinary SU UMa-type systems. These authors argued that the 2018 superoutburst was associated with the extension of the accretion disk falling short of the 2:1 resonance because of a reduced amount of mass in the disk. EG Cnc underwent a normal outburst in 2009, which could have depleted its disk mass. Hence, they considered the initial decay in the light curve to be a precursor to the superoutburst.

We speculate that the current superoutburst of 2020iko may be similar to the 2015 superoutburst of AL Com and 2018 superoutburst of EG Cnc (provided the initial decay in its light curve was indeed a precursor), where the accretion disk expanded just up to the 3:1 resonance radius. Then, the large decay of 3–5 mag in the precursor of 2020iko indicates a relatively slow growth of the tidal instability, which powers the main outburst. Direct evidence of tidal instability would have been provided by high-cadence (minute-scale) observations in this decay branch (as was the case for V1504 Cyg and V644 Lyr observed with Kepler), which unfortunately are not available for this source. The growth rate of this particular tidal instability is proportional to q^2 , where q is the mass ratio of the system (Osaki 1995). WZ Sge systems are characterized by very low values of q (typically 0.07–0.08; Kato 2015). Thus, the large decay of 2020iko’s precursor would imply that its mass ratio is extremely small—possibly smaller than that of EG Cnc, for which $q \sim 0.048$ (Kimura et al. 2020). Detailed theoretical modeling of the multiband light curves of 2020iko is beyond the scope of this paper, however, such work would help to provide insight into its extreme characteristics and throw light on why such precursors are rare in these low- q systems.

5. Conclusion

We report the first result from a successful beta implementation of the anomaly detection algorithm of Soraisam et al. (2020b) in the real-time alert environment within ANTARES. 2020iko, located close to an extended source, was flagged from the ZTF public alert stream as a candidate peculiar source (see Figure 2). We undertook spectroscopic as well as photometric multiwavelength follow-up observations, in particular, using LCO and MITSuME facilities. The fully assembled light curve of 2020iko reveals a precursor, a main superoutburst, and rebrightenings, while the spectrum taken during the superoutburst exhibits a blue continuum with higher-order Balmer lines in absorption, typical of DNe. The precursor has an amplitude of 6.5 mag and the superoutburst, 7 mag. Based on ASAS-SN data, the source, however, has no historical outburst going back to 2014, pointing to a recurrence period of >6 yr. Taking together all these results, we conclude 2020iko to be a WZ Sge-type DN candidate. Its precursor outburst with a large amplitude of 6.5 mag and a decay spanning 3–5 mag is unprecedented for DNe. We speculate this event of 2020iko to be a superoutburst with a limited expansion of the accretion disk, falling within the 2:1 resonance radius reached in typical




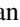






superoutbursts in other WZ Sge systems. Detailed theoretical modeling of the data presented here will help to throw light on the factors leading to atypical limited expansion of accretion disks in superoutbursts in WZ Sge-type DNe.

We thank the referee for the helpful comments that have helped improve the paper. This work makes use of observations from the LCO network. M.D.S. is supported by the Illinois Survey Science Fellowship of the Center for Astrophysical Surveys at the University of Illinois at Urbana-Champaign. D.J. S. acknowledges support from NSF AST-1813466. This work was supported in part by Grant-in-Aid for Scientific Research on Innovative Areas (17H06362), Optical and Near-Infrared Astronomy Inter-University Cooperation Program, and the joint research program of the Institute for Cosmic Ray Research (ICRR).

Facilities: LCO, Swift (XRT and UVOT).

Software: numpy (van der Walt et al. 2011), scipy (Jones et al. 2001), astropy (Astropy Collaboration et al. 2013), matplotlib (Hunter 2007), HEASOFT (NASA High Energy Astrophysics Science Archive Research Center 2014).

ORCID iDs

Monika D. Soraisam  <https://orcid.org/0000-0001-6360-992X>
 Chien-Hsiu Lee  <https://orcid.org/0000-0003-1700-5740>
 Thomas Matheson  <https://orcid.org/0000-0001-6685-0479>
 Gautham Narayan  <https://orcid.org/0000-0001-6022-0484>
 Abhijit Saha  <https://orcid.org/0000-0002-6839-4881>
 David J. Sand  <https://orcid.org/0000-0003-4102-380X>
 Carl Stubens  <https://orcid.org/0000-0002-2744-714X>
 Paula Szkody  <https://orcid.org/0000-0003-4373-7777>
 Nicholas Wolf  <https://orcid.org/0000-0002-9508-1629>
 Nobuyuki Kawai  <https://orcid.org/0000-0001-9656-0261>

References

- Alam, S., Albareti, F. D., Allende Prieto, C., et al. 2015, *ApJS*, 219, 12
 Astropy Collaboration, Robitaille, T. P., Tollerud, E. J., et al. 2013, *A&A*, 558, A33
 Barclay, T., Still, M., Jenkins, J. M., Howell, S. B., & Roettenbacher, R. M. 2012, *MNRAS*, 422, 1219
 Bellm, E. C., Kulkarni, S. R., Graham, M. J., et al. 2019, *PASP*, 131, 018002
 Brown, T. M., Baliber, N., Bianco, F. B., et al. 2013, *PASP*, 125, 1031
 Clarke, J. T., Capel, D., & Bowyer, S. 1984, *ApJ*, 287, 845
 Dai, Z., Szkody, P., Garnavich, P. M., & Kennedy, M. 2016, *AJ*, 152, 5
 Dey, A., Schlegel, D. J., Lang, D., et al. 2019, *AJ*, 157, 168
 Drake, A. J., Gänsicke, B. T., Djorgovski, S. G., et al. 2014, *MNRAS*, 441, 1186
 Förster, F., Cabrera-Vives, G., Castillo-Navarrete, E., et al. 2020, arXiv:2008.03303
 Gehrels, N., Chincarini, G., Giommi, P., et al. 2004, *ApJ*, 611, 1005
 Giles, D., & Walkowicz, L. 2019, *MNRAS*, 484, 834
 Green, G. M., Schlafly, E. F., Finkbeiner, D., et al. 2018, *MNRAS*, 478, 651
 Hameury, J.-M. 2020, *AdSpR*, 66, 1004
 NASA High Energy Astrophysics Science Archive Research Center 2014, HEASoft: Unified Release of FTOOLS and XANADU, v6.19, Astrophysics Source Code Library, ascl:1408.004
 Home, K., & Cook, M. C. 1985, *MNRAS*, 214, 307
 Howell, S. B., Henden, A. A., Landolt, A. U., & Dain, C. 2004, *PASP*, 116, 527
 Howell, S. B., Szkody, P., & Cannizzo, J. K. 1995, *ApJ*, 439, 337
 Hunter, J. D. 2007, *CSE*, 9, 90
 Ishida, E. E. O., Kornilov, M. V., Malanchev, K. L., et al. 2019, arXiv:1909.13260
 Ivezić, Ž., Kahn, S. M., Tyson, J. A., et al. 2019, *ApJ*, 873, 111
 Jayasinghe, T., Kochanek, C. S., Stanek, K. Z., et al. 2018, *MNRAS*, 477, 3145
 Jones, E., Oliphant, T., Peterson, P., et al. 2001, SciPy: Open Source Scientific Tools for Python, <http://www.scipy.org/>
 Kato, T. 2015, *PASJ*, 67, 108
 Kato, T., Monard, B., Hamsbich, F.-J., Kiyota, S., & Maehara, H. 2013, *PASJ*, 65, L11
 Kimura, M., Isogai, K., Kato, T., et al. 2016a, *PASJ*, 68, 55
 Kimura, M., Isogai, K., Kato, T., et al. 2020, *PASJ*, in press
 Kimura, M., Kato, T., Imada, A., et al. 2016b, *PASJ*, 68, L2
 Kochanek, C. S., Shappee, B. J., Stanek, K. Z., et al. 2017, *PASP*, 129, 104502
 Kotani, T., Kawai, N., Yanagisawa, K., et al. 2005, *NCimC*, 28, 755
 Lasota, J.-P. 2001, *NewAR*, 45, 449
 Lin, D. N. C., & Papaloizou, J. 1979, *MNRAS*, 186, 799
 Littlefield, C., Garnavich, P., Kennedy, M., Szkody, P., & Dai, Z. 2018, *AJ*, 155, 232
 LSST Science Collaboration, Marshall, P., Anguita, T., et al. 2017, arXiv:1708.04058
 Masci, F. J., Laher, R. R., Rusholme, B., et al. 2019, *PASP*, 131, 018003
 Matheson, T., Stubens, C., Wolf, N., et al. 2020, arXiv:2011.12385
 McCully, C., Volgenau, N. H., Harbeck, D.-R., et al. 2018, *Proc. SPIE*, 10707, 107070K
 Meyer, F., & Meyer-Hofmeister, E. 1981, *A&A*, 104, L10
 Mróz, P., Udalski, A., Poleski, R., et al. 2015, *AcA*, 65, 313
 Nogami, D., & Iijima, T. 2004, *PASJ*, 56, S163
 Nordin, J., Brinnet, V., van Santen, J., et al. 2019, *A&A*, 631, A147
 Osaki, Y. 1995, *PASJ*, 47, 47
 Osaki, Y. 1996, *PASP*, 108, 39
 Osaki, Y., 2014, *PASJ*, 66, 15
 Osaki, Y., & Kato, T. 2013, *PASJ*, 65, 50
 Osaki, Y., & Meyer, F. 2002, *A&A*, 383, 574
 Osaki, Y., & Meyer, F. 2003, *A&A*, 401, 325
 Pala, A. F., Gänsicke, B. T., Breedt, E., et al. 2020, *MNRAS*, 494, 3799
 Patterson, J., Kemp, J., Skillman, D. R., et al. 1998, *PASP*, 110, 1290
 Patterson, M. T., Bellm, E. C., Rusholme, B., et al. 2019, *PASP*, 131, 018001
 Saha, A., Wang, Z., Matheson, T., et al. 2016, *Proc. SPIE*, 9910, 99100F
 Shakura, N. I., & Sunyaev, R. A. 1973, *A&A*, 500, 33
 Shappee, B. J., Prieto, J. L., Grupe, D., et al. 2014, *ApJ*, 788, 48
 Smak, J. 1971, *AcA*, 21, 15
 Smak, J. 1993, *AcA*, 43, 101
 Smith, K. W., Williams, R. D., Young, D. R., et al. 2019, *RNAAS*, 3, 26
 Soraisam, M., Lee, C.-H., Narayan, G., Matheson, T., & Saha, A. 2020a, *ATel*, 13706, 1
 Soraisam, M. D., Saha, A., Matheson, T., et al. 2020b, *ApJ*, 892, 112
 Szkody, P., Anderson, S. F., Agüeros, M., et al. 2002, *AJ*, 123, 430
 Szkody, P., D'Amico, B., Ho, A. Y. Q., et al. 2020, *AJ*, 159, 198
 Szkody, P., Fraser, O., Silvestri, N., et al. 2003, *AJ*, 126, 1499
 Tonry, J. L., Denneau, L., Heinze, A. N., et al. 2018, *PASP*, 130, 064505
 Uemura, M., Arai, A., Krajci, T., et al. 2008, *PASJ*, 60, 227
 Valenti, S., Sand, D., Pastorello, A., et al. 2014, *MNRAS*, 438, L101
 van der Walt, S., Colbert, S. C., & Varoquaux, G. 2011, *CSE*, 13, 22
 Véron-Cetty, M. P., & Véron, P. 2010, *A&A*, 518, A10
 Warner, B. 2003, *Cataclysmic Variable Stars* (Cambridge: Cambridge Univ. Press)
 Whitehurst, R. 1988, *MNRAS*, 232, 35
 Wood, M. A., Still, M. D., Howell, S. B., Cannizzo, J. K., & Smale, A. P. 2011, *ApJ*, 741, 105